

## Supporting Information

### **High-Performance Triboelectric Nanogenerator Employing Swing-Induced Counter-Rotating Motion Mechanism and Dual Potential Energy Storage and Release Strategy for Wave Energy Harvesting**

Feixiang Wang<sup>a</sup>, Bao Cao<sup>c</sup>, Leilei Shu<sup>a</sup>, Zhe Li<sup>a</sup>, Wen He<sup>a</sup>, Zhongzhu Wang<sup>a</sup> and Peihong Wang<sup>a, b, \*</sup>

<sup>a</sup> School of Materials Science and Engineering, Energy Materials and Devices Key Lab of Anhui Province for Photoelectric Conversion, Anhui University, Hefei, Anhui 230601, China

<sup>b</sup> Key Laboratory of Structure and Functional Regulation of Hybrid Materials, Anhui University, Ministry of Education, Hefei, Anhui 230601, China

<sup>c</sup> Academy of Engineering and Technology, Fudan University, Shanghai 200433, China

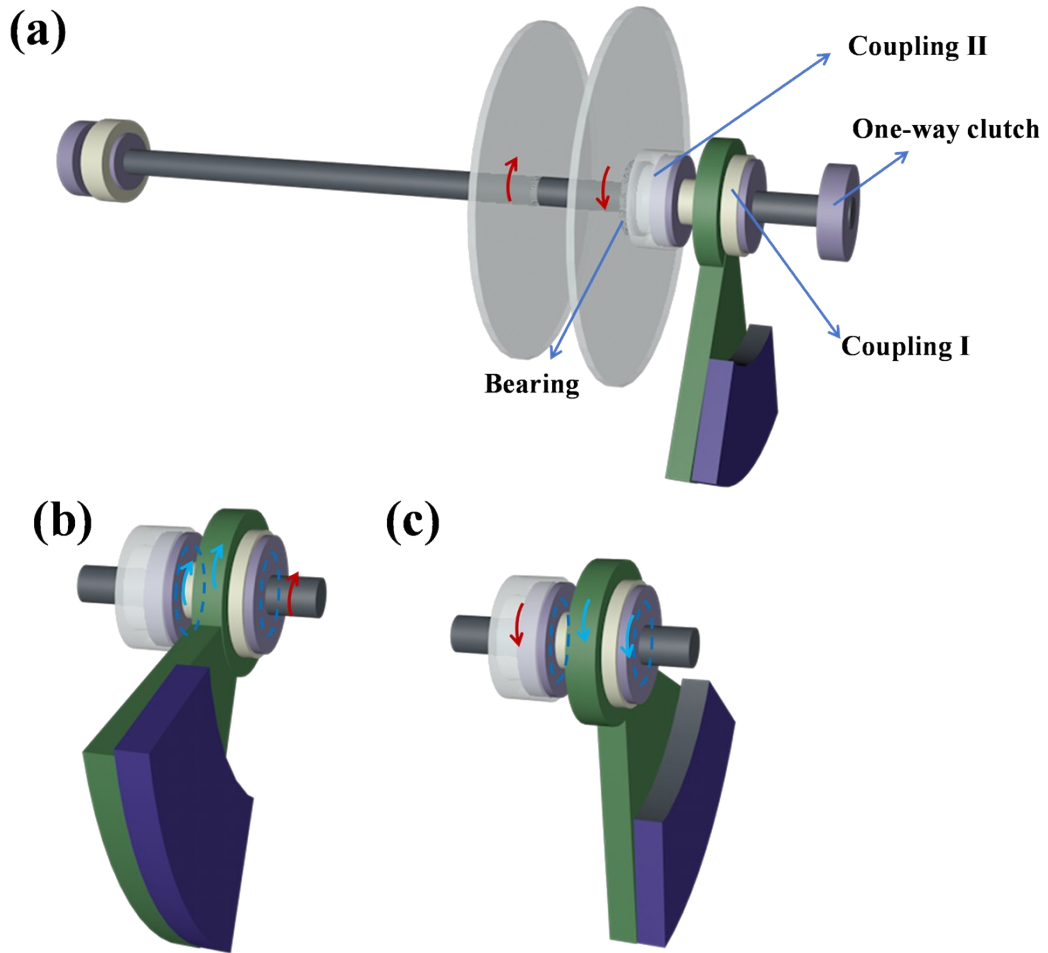


**Figure S1.** Schematic diagram of components of SD-TENG. a) The multi-bearing center rod structure is mainly composed of a center rod, two swing-induced counter-rotating structures (SCS), a one-way clutch, and a bearing. b) The pendulum swings clockwise, the center rod of the SCS structure drives the inner cylinder to rotate clockwise. c) The pendulum rotates counterclockwise, the SCS structure and another coupling II connected to the outer cylinder drive the outer cylinder to rotate counterclockwise.

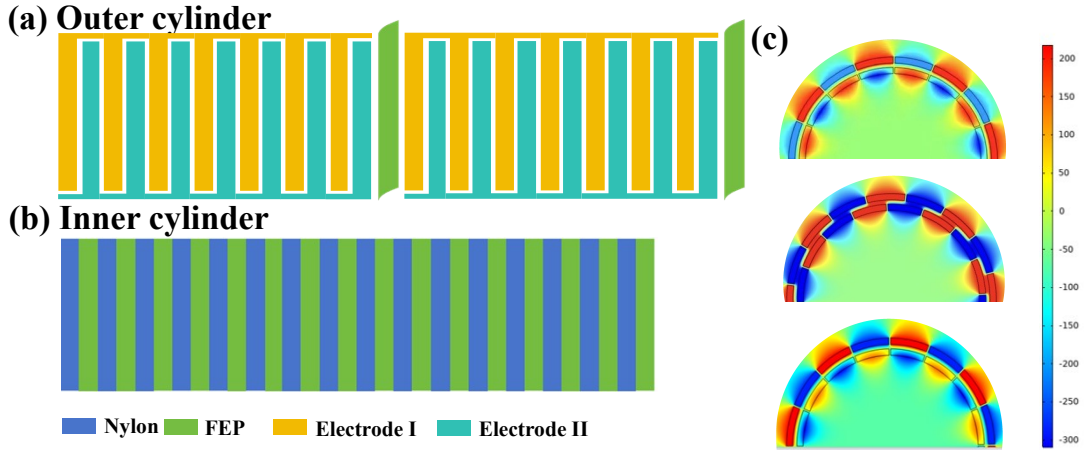


**Figure S2.** The physical diagram of a) the electrode layer, charge pump and b) two dielectric films. c) The results of COMSOL Multiphysics software.

**Note S1 for the Figure 2c:** The external force and acceleration provided to the outer pendulum by the external environment can be expressed as follows (where  $\omega = 2\pi f$ ):

$$F = m_I a \quad \text{S1}$$

$$a = \omega^2 A \cos(\omega t) \quad \text{S2}$$

Among them, the mass of mass block I is represented by  $m_I$ , the excitation frequency is  $f$ , the excitation amplitude is  $A$ , and the forced vibration time is  $t$ .

**Note S2 for the Figure 2c:** Based on the functional principle,  $W_F$  can also be expressed in terms of the energy loss within the mechanical structure and the potential energy transferred to the mass block II or mass block III. The corresponding formula are as following:

$$\begin{aligned} W_F &= W_{1f} + W_{2f} + \Delta E_{p2} = W_{1f} + W_{2f} + m_{II} g l_{II} (\cos \alpha_g - \cos \alpha_3) \\ &= W_{1f} + W_2 \end{aligned} \quad \text{S3}$$

$$\begin{aligned} W_F &= W_{1f} + W_{3f} + \Delta E_{p3} = W_{1f} + W_{3f} + m_{III} g l_{III} (\cos \beta_g - \cos \beta_3) \\ &= W_{1f} + W_3 \end{aligned} \quad \text{S4}$$

As for formula S3,  $W_{1f}$  represents the energy loss of the swing component due to friction,  $W_{2f}$  stands for the energy loss of the mass block II,  $\Delta E_{p2}$  is the potential energy difference of the mass block II,  $l_{II}$  represents the distance

between the central axis and mass block II.  $W_2$  is the overall energy of mass block II.

As for formula S4,  $W_{1f}$  represents the energy loss of the swing component due to friction,  $W_{3f}$  indicates the energy loss of the mass block III,  $\Delta E_{p3}$  is the potential energy difference of the mass block III,  $l_{III}$  denotes the distance between the central axis and mass block III. And  $W_3$  is the overall energy of mass block III.



Mass

**Figure S3.** The schematic diagram of the definition of  $\theta$ ,  $\alpha$  and  $\beta$ .

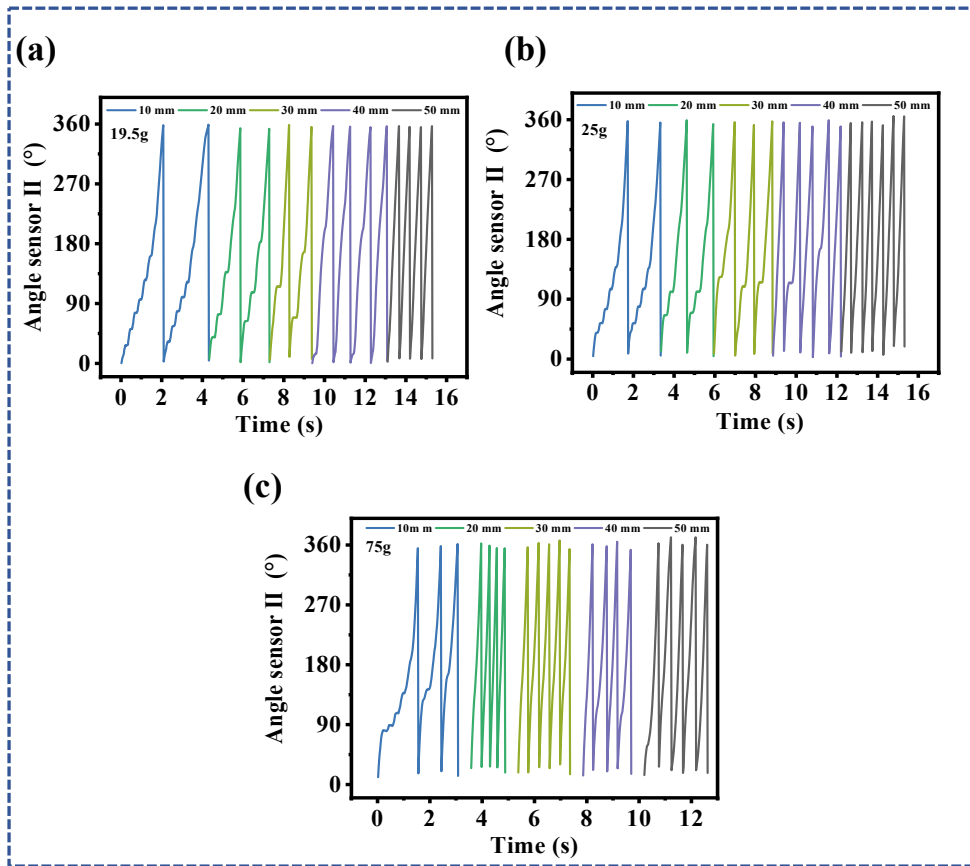


**Figure S4.** The angle curve of the outer cylinder when the mass of mass III is changed to 19.5 g, 25 g and 75 g respectively.

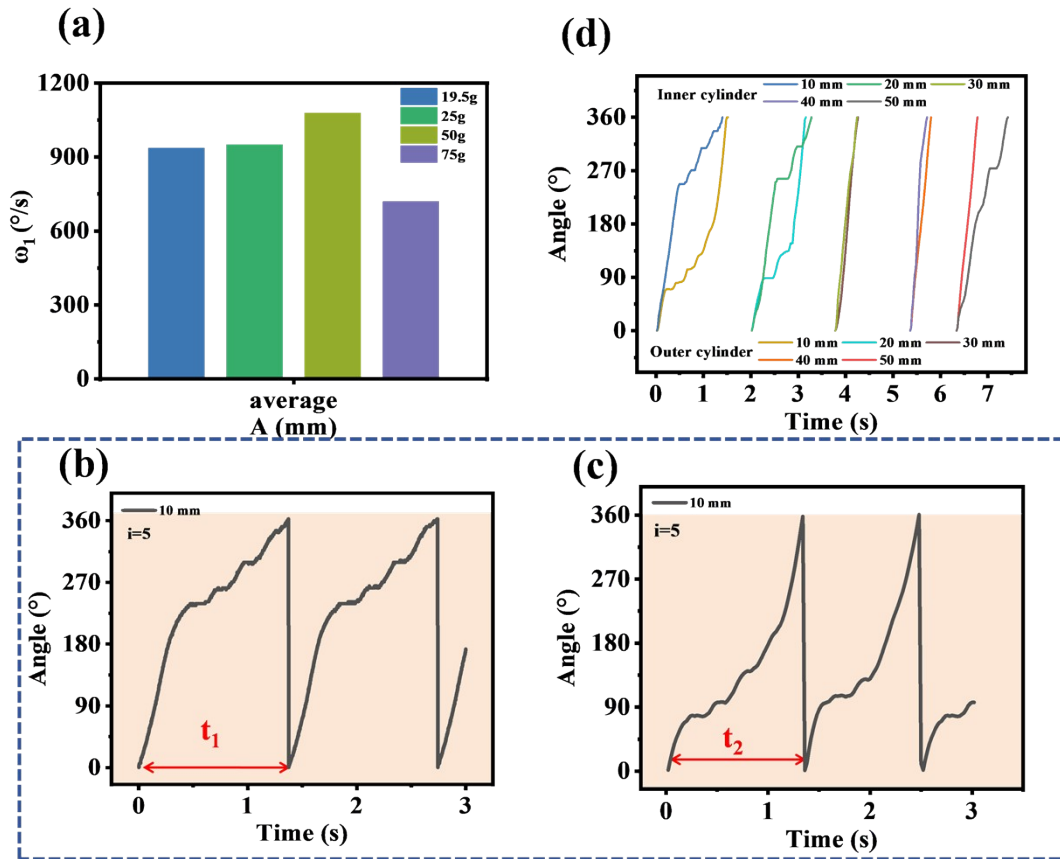


**Figure S5.** a) The average angular velocity of the outer cylinder under 10-50 mm. The schematic diagram of the definition of b)  $t_1$  and c)  $t_2$ . d) The angle of the inner and outer cylinders of SD-TENG under the optimal optimization condition.

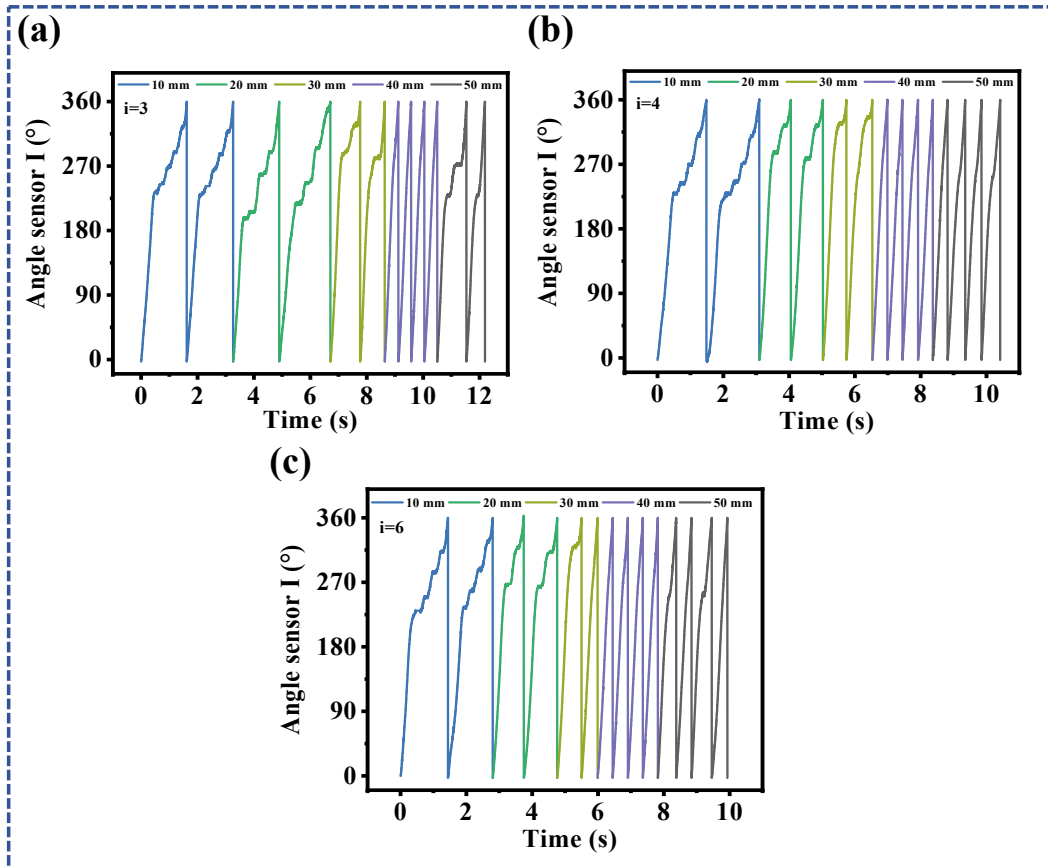


**Figure S6.** The angle curve of the inner cylinder under the mass ratio  $i = 3, 4, 6$ .

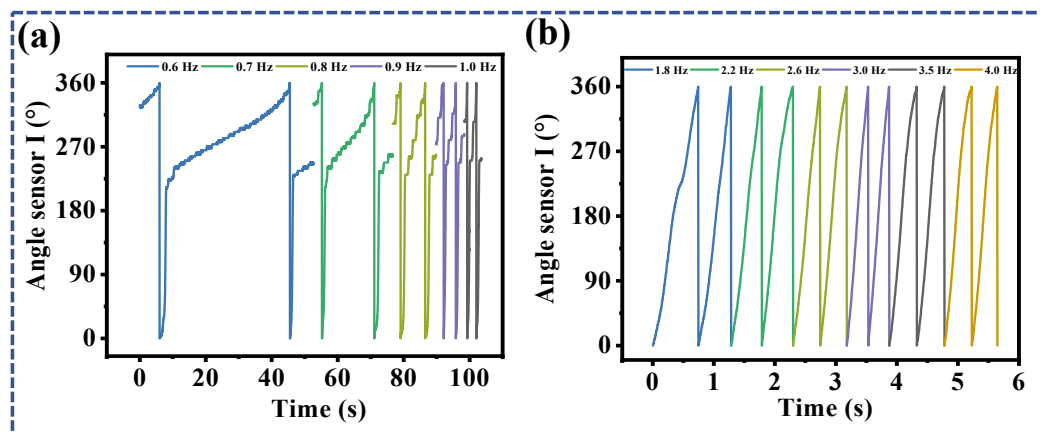


**Figure S7.** The angle data of the inner cylinder at very low frequencies (less than 1 Hz) and high frequencies (1.8 - 4 Hz).

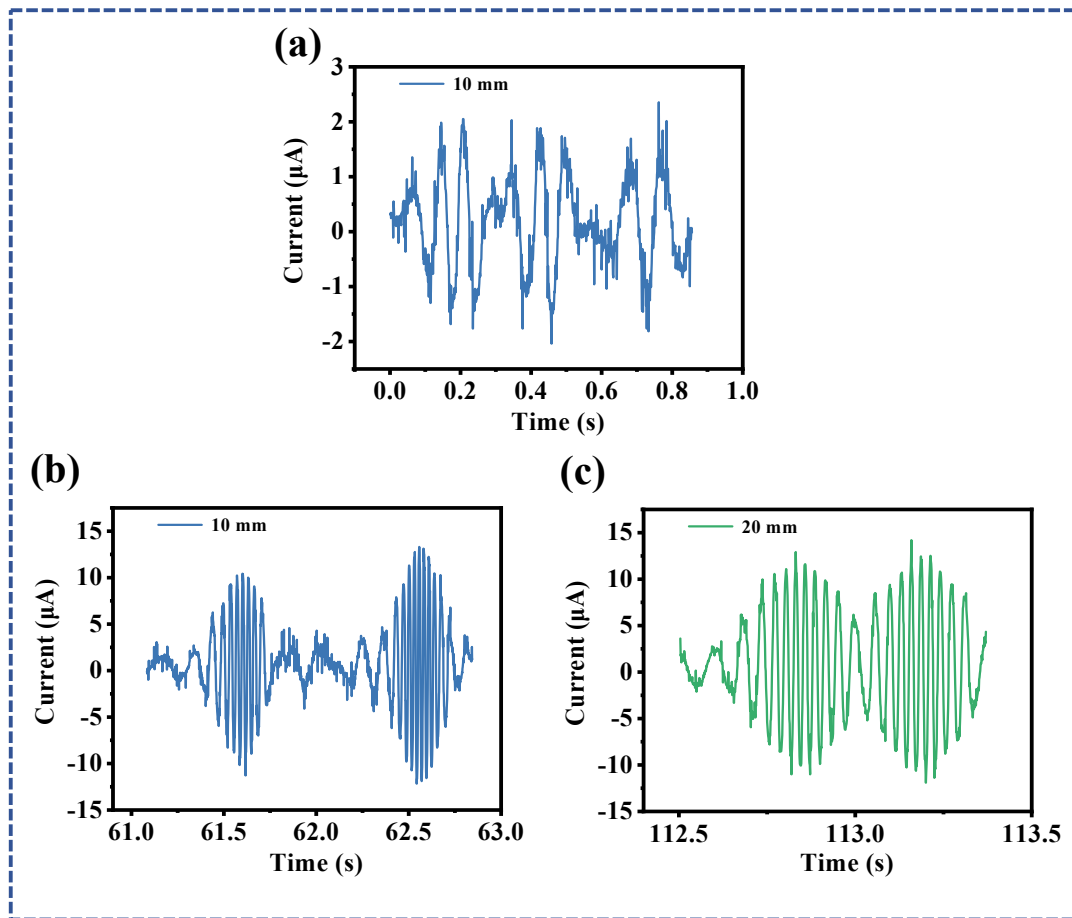


**Figure S8.** (a) The curve of output in the potential energy accumulation stage. The specific peak current conditions of b) 10 mm and c) 20 mm.



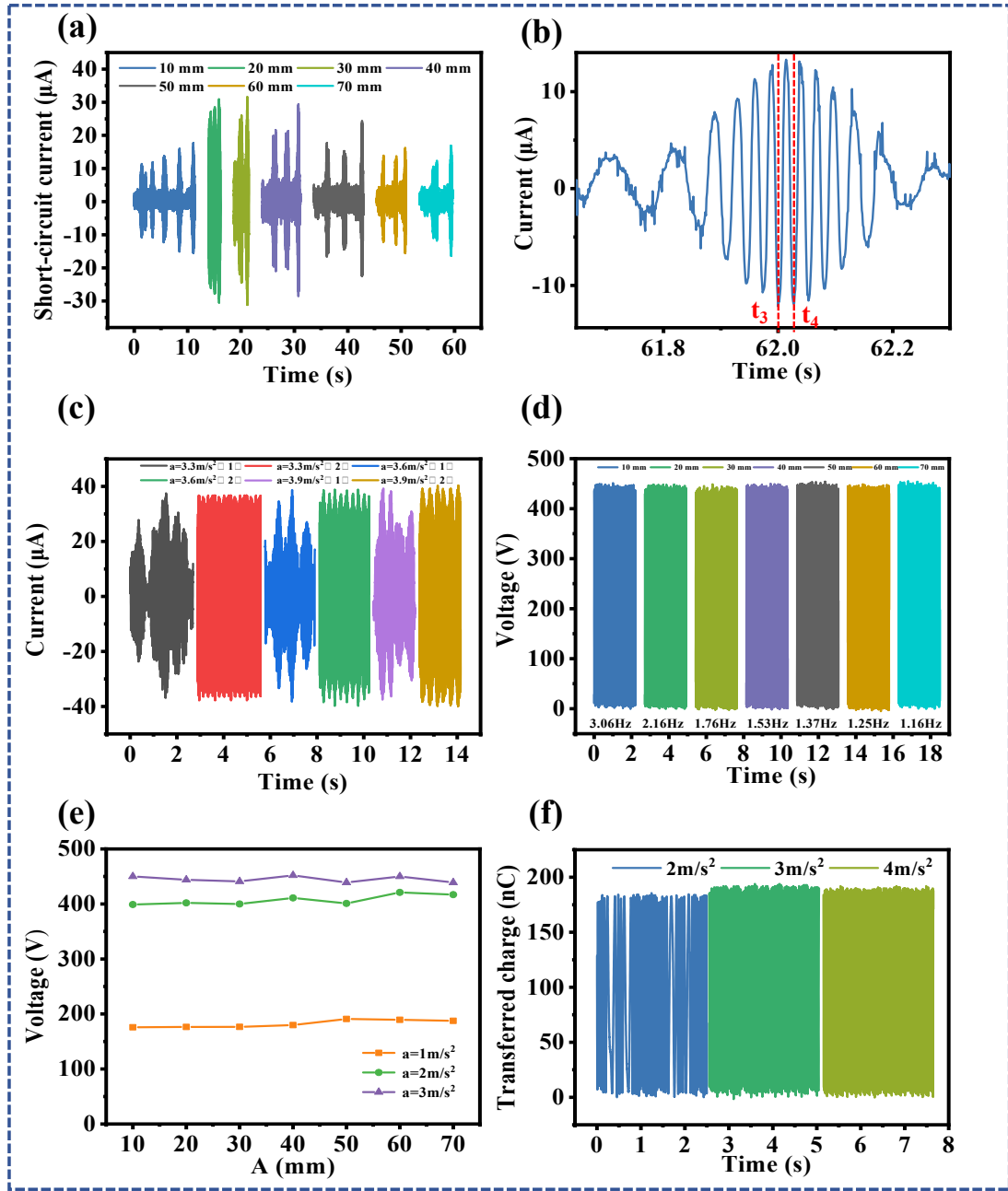


**Figure S9.** a) The current output at acceleration  $a = 2$   $\text{m/s}^2$ ,  $A = 10$ - $70$  mm. b) The schematic diagram of the definition of  $t_3$  and  $t_4$ . c) The current output of SD-TENG in two different modes with  $A = 30$  mm,  $a = 3.3$   $\text{m/s}^2$ ,  $a = 3.6$   $\text{m/s}^2$  and  $a = 3.9$   $\text{m/s}^2$ . d) The voltage output at acceleration  $a = 3$   $\text{m/s}^2$ ,  $A = 10$  -  $70$  mm. e) The relationship between the peak voltage of SD-TENG and the amplitude. f) The transferred charge ( $Q_{sc}$ ) under different excitation  $a = 2$  -  $4$   $\text{m/s}^2$  and fixed  $A = 30$  mm.

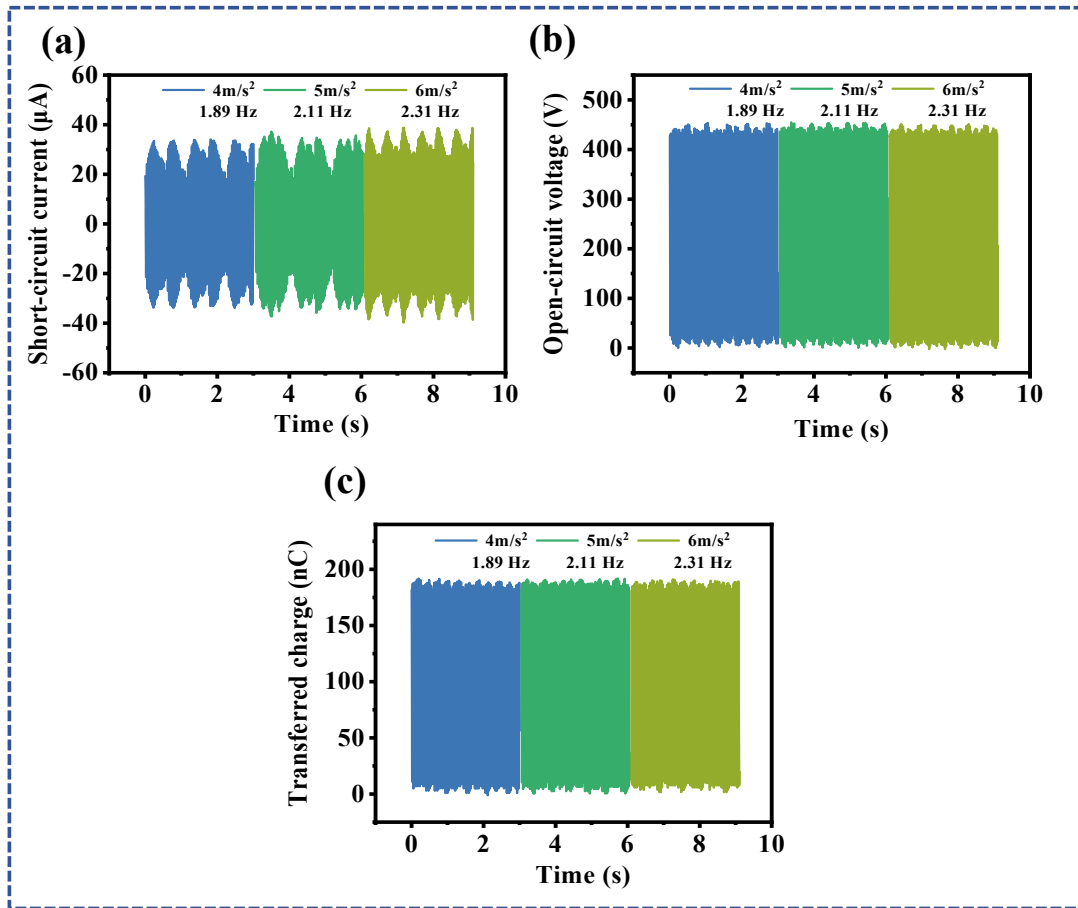


**Figure S10.** The measurement results of SD-TENG short-circuit current ( $I_{sc}$ ), open circuit voltage ( $V_{oc}$ ) and transferred charge ( $Q_{sc}$ ) at  $a = 4\text{--}6\text{ m/s}^2$  and fixed  $A = 35\text{ mm}$ .

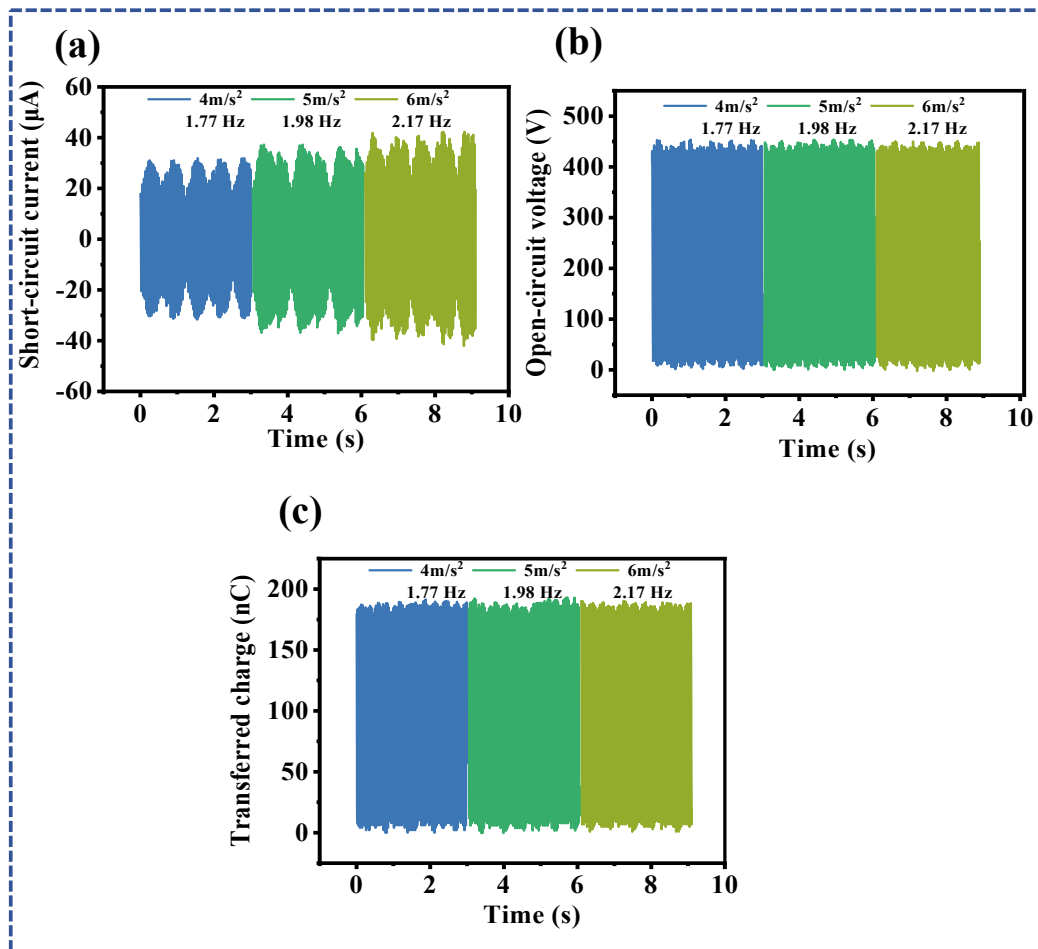


**Figure S11.** The measurement results of SD-TENG short-circuit current ( $I_{sc}$ ), open circuit voltage ( $V_{oc}$ ) and transferred charge ( $Q_{sc}$ ) at  $a = 4-6 \text{ m/s}^2$  and fixed  $A = 40 \text{ mm}$ .

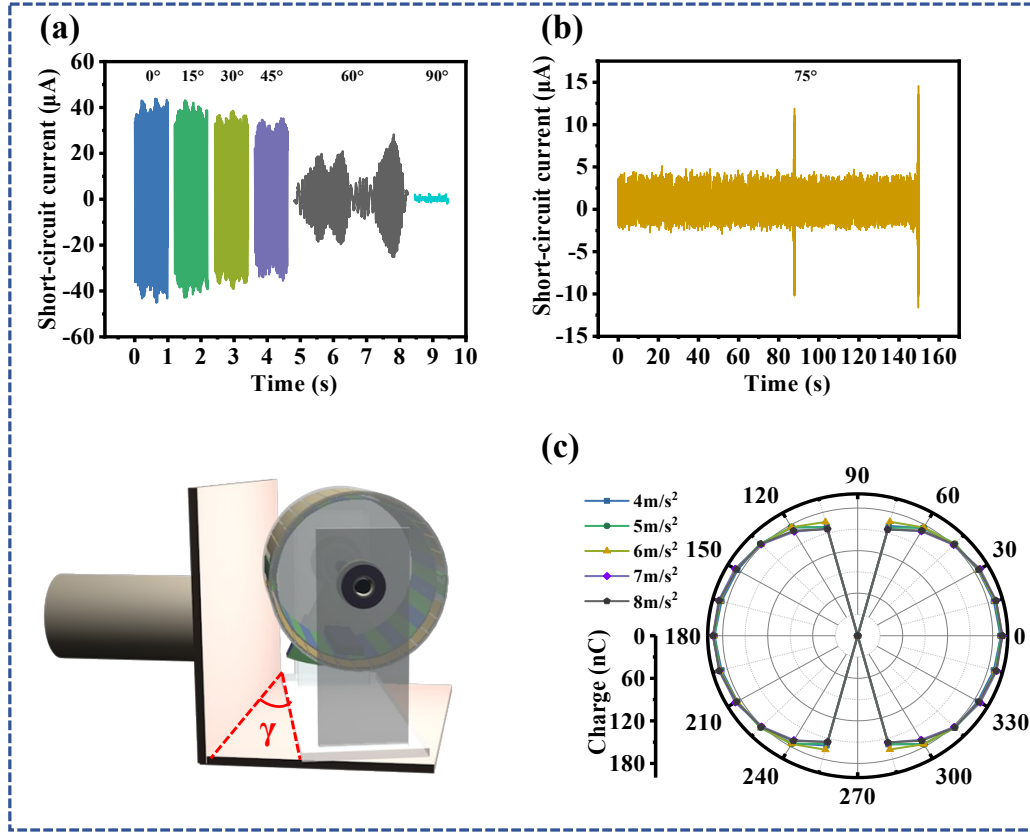


**Figure S12.** The ability of SD-TENG to collect low-frequency mechanical energy in different directions ( $I_{sc}$  in different directions). The dependence of (a) (b) short-circuit current and (c) transferred charge ( $Q_{sc}$ ) with the angle ranging from  $0^\circ$  to  $90^\circ$  under  $a = 6 \text{ m/s}^2$   $A = 30 \text{ mm}$ .

**Note S3.** As shown in formula S5 below, we calculated its energy conversion efficiency to be 19.46% under the conditions of  $a = 5 \text{ m/s}^2$  and  $A = 30 \text{ mm}$  (the input energy was 95 mJ, the output energy was 18.49 mJ, and the dissipated energy was 76.51 mJ). We measured the torque of the SD-TENG 15 mN·m using a torque sensor, and calculated the frictional force of the charge pump to be 125N according to formula S6 below. Subsequently, we calculated the energy loss due to frictional resistance to be 11.8 mJ. The dissipated energy is mainly distributed between the energy lost due to friction and the energy lost due to mechanical damping. We can obtain that the energy due to mechanical damping is 64.71 mJ, accounting for 68.11% of the total energy. Since the friction materials are in soft contact through a charge pump, the frictional resistance is greatly reduced, and thus the energy loss due to frictional resistance is relatively small. The energy loss due to mechanical damping is relatively large and has a significant impact on the overall energy conversion efficiency.

$$\eta = \frac{E_{out}}{E_{in}} = \frac{\int_0^T I(t)^2 R d\theta}{2(m_{II} g l_{II} + m_{III} g l_{III})}$$

$$F_r = \frac{M}{r}$$

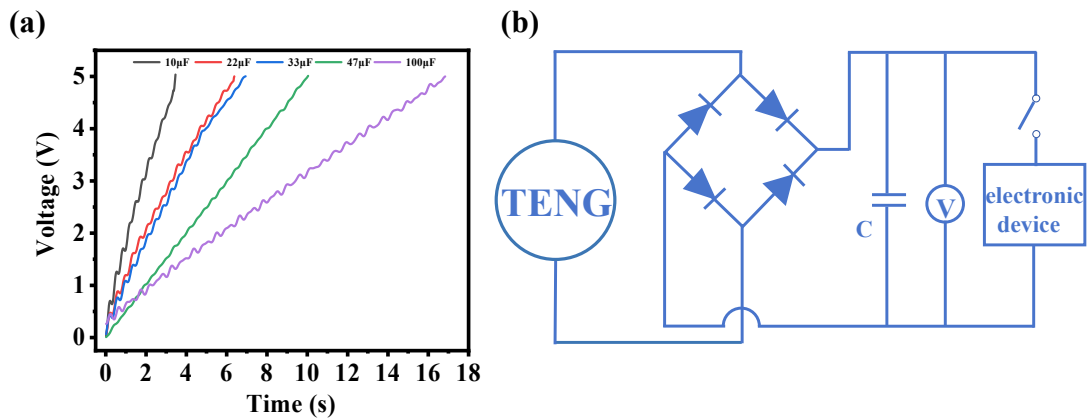


**Figure S13.** a) The charging capacity of SD-TENG at  $a = 8 \text{ m/s}^2$  and  $A = 30 \text{ mm}$ . b) The circuit diagram for driving the small electronic device.

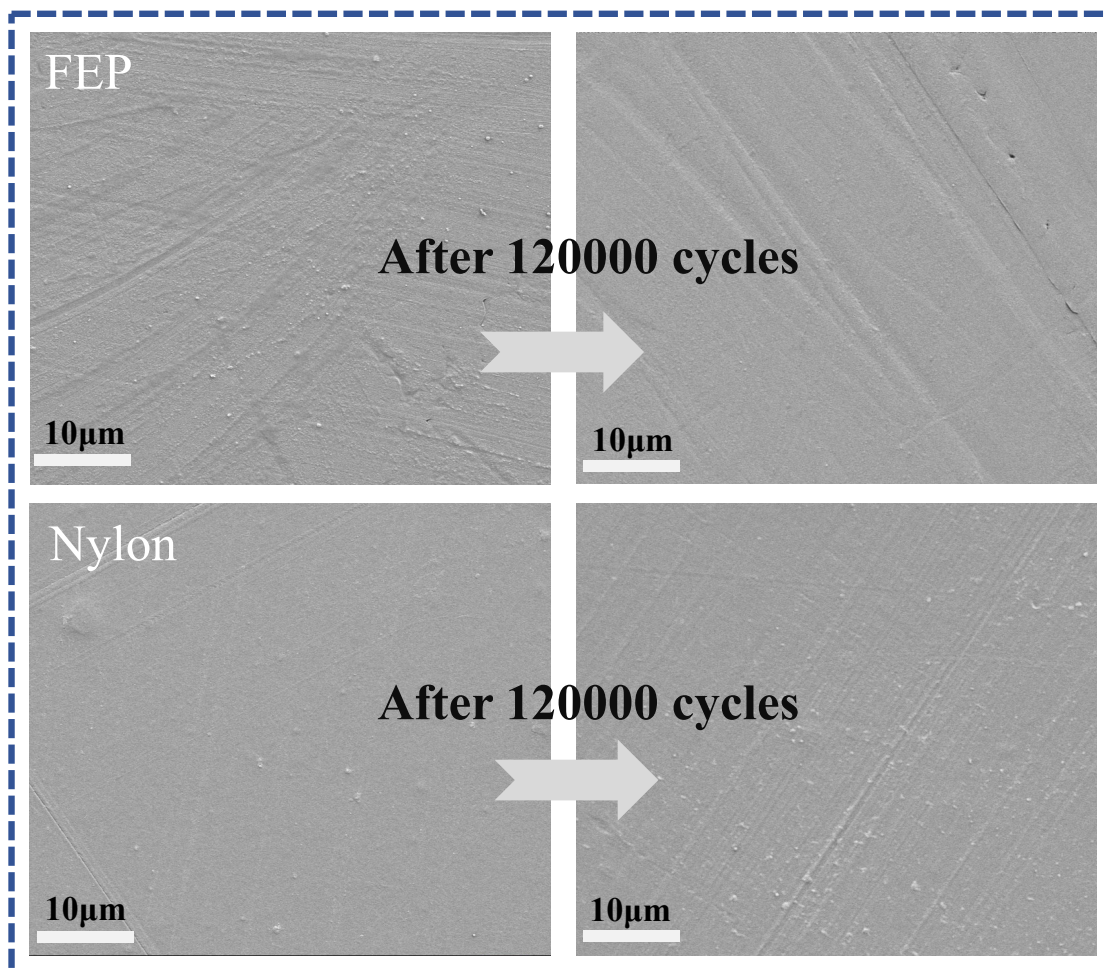


**Figure S14.** The SEM images of the two films on the inner cylinder before and after 120000 cycles of testing.